ACUSTICA
Vol. 79 (1993)



# Idealised Models of a Bowed String

J. Woodhouse
Cambridge University Engineering Department, Cambridge, UK

**Idealised Models of a Bowed String**

**Summary**

Several idealised models for the self-excited oscillation of a bowed string are studied and compared: Raman's and Friedlander's models, in which boundary reflections are described by frequency-independent reflection coefficients, and the rounded-corner models in which the process of reflection is characterised by two "reflection functions". The rich set of possible periodic solutions is explained, and computational methods are given for calculating them. Implications for the limits of allowed normal force between bow and string are explored. Finally, the limiting processes are studied, by which the predictions of the Raman model and the rounded-corner models might be expected to tend towards those of the Friedlander model. Both of these limits show unexpected behaviour, an understanding of which is vital to any modelling exercise making use of the Raman and Friedlander models.

**Idealisierte Modelle einer gestrichenen Saite**

**Zusammenfassung**

Es werden verschiedene idealisierte Modelle für die selbsterregte Schwingung einer angestrichenen Saite untersucht und verglichen: Die Modelle von Raman und Friedlander, bei denen die Reflexionen von den Saitenenden durch frequenzunabhängige Reflexionskoeffizienten beschrieben werden, und die Modelle der „abgerundeten Ecken", bei denen der Reflexionsprozeß durch zwei Reflexionsfunktionen gekennzeichnet wird. Der große Satz möglicher periodischer Lösungen wird erklärt und es werden Berechnungsmethoden für sie angegeben. Außerdem werden Folgerungen für die Grenzen der zulässigen Normalkraft zwischen Bogen und Saite untersucht. Schließlich werden die Grenzprozesse studiert, aufgrund derer die Vorhersagen des Raman-Modells und des Modells der abgerundeten Ecken in die des Friedlander-Modells übergehen könnten. Beide derartige Grenzen zeigen ein unerwartetes Verhalten, dessen Verständnis von großer Bedeutung für jede Modelluntersuchung auf der Grundlage des Raman- und Friedlander-Modells ist.

**Modèles idéalisés d'une corde frottée**

**Sommaire**

Nous procédons à une analyse comparée de plusieurs modèles idéalisés du mécanisme d'auto-excitation des vibrations d'une corde frottée: les modèles de Raman et de Friedlander, dans lesquels les réflexions aux extrémités sont représentées par des coefficients de réflexion indépendants de la fréquence, et les modèles «à angles arrondis» où les mécanismes de réflexion sont caractérisés par deux «fonctions de réflexion». On explique le riche éventail des solutions périodiques possibles, et l'on indique des méthodes pour leur calcul. On examine les conséquences sur les limites acceptables de la force normale de l'archet sur la corde. Finalement on étudie les cas limites où l'on peut prévoir que les résultats du modèle de Raman et ceux des modèles à angles arrondis peuvent tendre vers les résultats du modèle de Friedlander. On découvre un comportement inattendu de ces cas limites, dont la compréhension est fondamentale pour l'utilisation des modélisations de Raman et de Friedlander.

## 1. Introduction

If asked to consider the behaviour of a bowed string, most applied mathematicians find one particular mathematical model immediately plausible. An ideal, perfectly flexible, stretched string is rigidly anchored at both ends. Excitation by bowing is modelled as a force applied at a single point of the string, the value of the force depending on the motion of the string at that point according to some non-linear relation representing stick-slip friction. This model has been studied in the past, especially by Friedlander [1] and Keller [2], and we shall refer to it as the "Friedlander model". A close relative of this model, although actually earlier, is due to Raman [3]. This differs from Friedlander's model in that the string terminations, instead of being rigid, have reflection coefficients with a magnitude less than unity, representing some energy dissipation. (Physically, it can be regarded as modelling string terminations which are pure mechanical resistances, or semi-infinite ideal strings whose wave impedances differ from that of the finite length of "actual" string.)

Although more sophisticated and accurate models have been available for some time now [4], the Friedlander and Raman models have the virtue of (appar-

Received 5 November 1992,
accepted 7 January 1993.

J. Woodhouse, Cambridge University Engineering Department, Trumpington Street, Cambridge CB2 1PZ, UK.

ent) simplicity, and they are still often invoked when explanations are sought for bowed-string phenomena. In this paper we explore the strengths and weaknesses of these models, to show when they give a useful guide to real bowed-string behaviour and when they can be seriously misleading. We will consider Friedlander's model as a limiting case of Raman's model, and also of the class of "rounded-corner models", in which a much wider class of wave reflection, dispersion and dissipation behaviour may be included [4–6]. In both cases we will find that the limit process is not straightforward, so that solutions to the Friedlander model do not generally give good approximations to the predictions of these other models, even close to the relevant limit.

In order to focus on the essential relations between these models, other aspects of the system will be approximated in the simplest possible way. In particular, the friction force will be modelled as depending only on the instantaneous string velocity at the bowed point. We will take a very simple piecewise-linear relation, illustrated as the heavy curve in Fig. 1. When the string has the same velocity $v_b$ as that of the "bow", there is sticking friction and the force may take any value between certain limits. This is represented by the vertical portion of the curve. When there is relative sliding, the friction force $f$ is assumed to vary according to

$$f/f_b = k v + c \tag{1}$$

where $v$ is the string velocity, $f_b$ the normal force between bow and string, and $k$ and $c$ are constants. For sliding speeds close to the bow speed, the straight line (1) is joined to the maximum of the sticking line by another straight line. In fact the form of this portion of the curve will not matter, as will be seen shortly. For sliding at speeds faster than $v_b$ the curve would be reproduced antisymmetrically, as shown in Fig. 1, but this does not occur in the usual motion of a bowed string and will not be considered further. This model does not represent real frictional behaviour very accurately [7], but it is a simple version of the most commonly-used model, and is well suited to the present investigation.

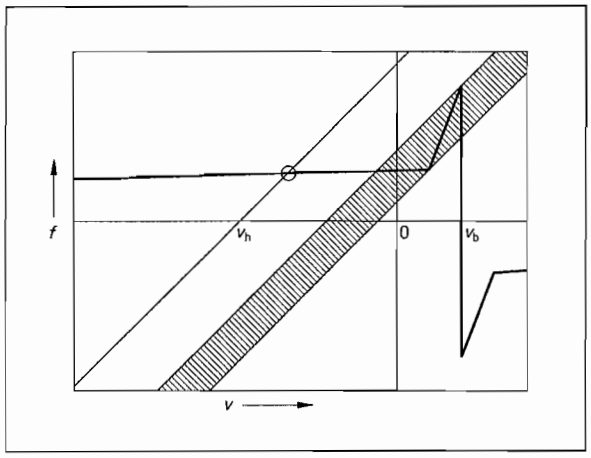


Fig. 1. The heavy curve shows a piecewise-linear relation between friction force and string velocity of the kind assumed throughout this paper. The sloping line and ringed intersection illustrate Friedlander's graphical procedure for finding the force and velocity at a given time step. The shaded region shows the range in which frictional hysteresis operates.

Friedlander first considered the solution which represents a state of steady sliding, in which the string does not vibrate but is simply held in a displaced position by a steady friction force. He argued that this solution must be unstable since it is never observed in a real violin string, and he showed that, within his model, a necessary and sufficient condition for this instability is that

$$k > 0 \tag{2}$$

in eq. (1). This condition, described by Schelleng [8] as "negative resistance", is necessary for self-excited oscillation to occur in any reasonable model on the simple friction-curve idealisation.

Friedlander's model has a periodic solution which corresponds quite well to the usual motion of a bowed string (first described by Helmholtz [9]), but he showed that eq. (2) is a sufficient condition for this and all other periodic solutions to be unstable, a conclusion which is not in good agreement with the common experience of violin playing. The nature of Friedlander's instability of the "Helmholtz motion" has been shown to take the form of subharmonic perturbations which grow exponentially [10]. His model lacks any mechanism of energy dissipation, whereas in a more realistic model subharmonic growth can be balanced by dissipation to give stable periodic motion. A more detailed discussion of this instability, and other questions relating to the stability of bowed-string motion, is given in a companion paper to this [11]. Here, we concentrate on the nature of the solutions to the different models, and their behaviour in various limiting cases.

## 2. Raman's model

### 2.1. Formulation and formal solutions

Raman's and Friedlander's models are sufficiently similar that it is convenient to develop them together. Suppose the string is of length $L$, divided into parts of lengths $a$ and $b$ by the bowed point. The reflection coefficients at the two ends of the string will be assumed to be the same, with value $-\lambda$. Since for any

reasonable model of a violin string boundary reflection will be almost complete, it is sometimes convenient to write $\lambda = 1 - \varepsilon$, where $\varepsilon$ will be a small positive number. In Friedlander's model, $\varepsilon = 0$. The velocity response at time $t$ at the bowed point is given straightforwardly in terms of the instantaneous force $f(t)$ and a sum of multiply-reflected contributions arising from forces applied by the bow at earlier times:

$$v(t) = (Y_0/2)\Big\{f(t) - \sum_{j=0}^{\infty} \lambda^{2j}[\lambda f(t - 2(a + jL)/c) + \lambda f(t - 2(b + jL)/c) - 2\lambda^2 f(t - 2(j+1)L/c)]\Big\} \quad (3)$$

where $Y_0$ is the characteristic admittance of the string, equal to $(Tm)^{-1/2}$ where $T$ is the string tension and $m$ its mass per unit length, and $c$ is the wave speed $\sqrt{T/m}$. It is convenient henceforth to use units in which $Y_0 = 2$.

If the bowed point is a rational subdivision of the string, eq. (3) reduces to a difference equation. Provided the initial conditions are consistent with the assumption, both $v(t)$ and $f(t)$ are piecewise constant functions. Suppose $a:b = p:q$ where $p$ and $q$ are co-prime integers with $p \leqq q$ for definiteness. Let

$$\Delta = 2L/cN$$

where $N = p + q$. Then eq. (3) may be written

$$v_n = f_n - \sum_{j=0}^{\infty} \lambda^{2j}[\lambda f_{n-p-jN} + \lambda f_{n-q-jN} - 2\lambda^2 f_{n-(j+1)N}] \quad (4)$$

where

$$v_n = v(n\Delta) \quad \text{and} \quad f_n = f(n\Delta).$$

By simple manipulation, eq. (4) may be cast in the closed form

$$f_n - \lambda f_{n-p} - \lambda f_{n-q} + \lambda^2 f_{n-N} = v_n - \lambda^2 v_{n-N} \quad (5)$$

which, for the case $\lambda = 1$, is the form used by Friedlander [1].

Eq. (5) gives a basis for a simple time-stepping calculation of transient response of the model. At a given time $n$, all terms except $v_n$ and $f_n$ are known from the past history of the motion, and these quantities enter in a simple linear manner which may be written in the form

$$v_n = f_n + v_h \quad (6)$$

where $v_h$ is known. The unknown quantities $v_n$ and $f_n$ may thus be found by solving eq. (6) simultaneously with the friction relation. This is conveniently visualised as the graphical construction shown in Fig. 1: the intersection of the straight line (6) with the friction curve is found, and its $x$ and $y$ coordinates are $v_n$ and $f_n$ respectively. It is clear that an ambiguity of intersections can arise if the line falls in the area shown shaded in the figure, and it has been shown that the physically correct resolution of this ambiguity involves a hysteresis cycle [12], as one might have guessed. The appropriate intersection to choose is whichever of the two outer ones corresponds to the state (sticking or slipping) of the previous time step. The middle intersection is never to be used, so that the precise assumed form for the friction curve in this region is immaterial. The limits of this shaded region will play a role when we seek periodic solutions to the model: they impose self-consistency constraints on allowable solutions.

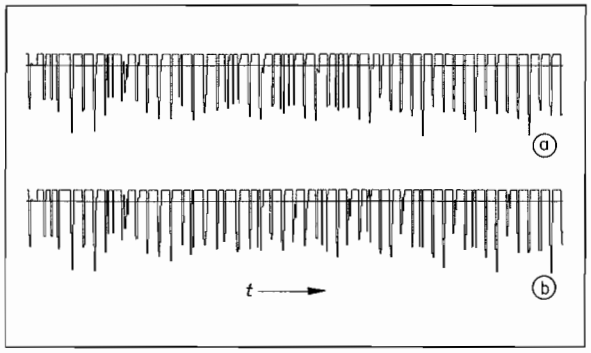


Fig. 2. Simulated transient solutions to a) Raman's model and b) Friedlander's model, from quiescent initial conditions at the left-hand side of the plots. Parameters used were: $p = 2$, $q = 9$, $f_b = 7$, $v_b = 1$, $k = 0.005$, $c = 0.3$, coefficient of sticking friction 0.8, maximum velocity on sliding portion of friction curve 0.8. For case a), the boundary reflection coefficients were both 0.99. In both cases, the waveform of string velocity at the bowed point is plotted.

Little progress can be made analytically in the study of transient solutions, even with the very simple friction law assumed here. It is, however, easy to compute examples, and two are shown in Fig. 2. Both start with the string at rest at time zero. The same values $p = 2$, $q = 9$ are used in both cases, and the only difference is in the assumed value of $\lambda$. Fig. 2a shows Raman's model with $\lambda = 0.99$, while Fig. 2b shows Friedlander's model, with $\lambda = 1$. The two models give similar results initially, but diverge after a short time. Friedlander's model shows no pattern (since all periodic solutions are unstable), but Raman's model eventually settles towards a periodic solution which approximates the Helmholtz motion. This has the period of the free motion of the string, and within each cycle it has one episode of slipping for $p$ time steps and one of sticking for $q$ time steps. This pattern is just starting to form by the end of the time range plotted, but it has a strong perturbation which is approximately a fifth subharmonic [10, 11]. This perturbation dies down slowly over the next 200 period-lengths or so. Neither transient bears very much resemblance to typical transients for normal playing of a real violin string, but

ACUSTICA
Vol. 79 (1993)

that is not an issue to be examined in this paper. A more systematic use of simulation to study the transient behaviour of bowed-string models has been discussed elsewhere [6].

We learn more about the relation between Friedlander's and Raman's models by looking at possible periodic solutions. Consider first the simplest case, in which the period is the natural period of free vibration of the string, and there is one slipping episode per cycle. We need not assume that it is a Helmholtz motion, with precisely $p$ slipping points – we assume some number which we denote $r$. The set of $N$ simultaneous equations which follow from eq. (5) together with the known relations between $f_n$ and $v_n$ during sticking and slipping may be written

$$\left(\frac{\boldsymbol{v}_\mathrm{b}}{\boldsymbol{v}}\right) = \frac{1}{1-\lambda^2}\begin{pmatrix} 1+\lambda^2 & & -\lambda & & -\lambda & & \\ & 1+\lambda^2 & & -\lambda & & & \\ -\lambda & & \ddots & & \ddots & & -\lambda \\ & & & \ddots & & & -\lambda \\ -\lambda & & \ddots & & \ddots & & \\ & & -\lambda & & -\lambda & & 1+\lambda^2 \end{pmatrix}\left(\frac{\boldsymbol{f}}{f_\mathrm{b}[k\boldsymbol{v}+\boldsymbol{c}]}\right) \tag{7}$$

where $\boldsymbol{v}$ is a vector of $r$ unknown velocities (during slipping), $\boldsymbol{f}$ a vector of $N-r$ unknown forces (during sticking), and $\boldsymbol{v}_\mathrm{b}$ and $\boldsymbol{c}$ are vectors filled with the corresponding scalar constants, of lengths $N-r$ and $r$ respectively. The diagonal lines of terms $-\lambda$ start in columns $(p+1)$ and $(q+1)$ of the first row, and the matrix is symmetric. All entries not otherwise indicated are zero.

The matrix may now be partitioned to match the partition of the vectors:

$$\left(\frac{\boldsymbol{v}_\mathrm{b}}{\boldsymbol{v}}\right) = \left(\begin{array}{c|c} \boldsymbol{A} & \boldsymbol{B} \\ \hline \boldsymbol{C} & \boldsymbol{D} \end{array}\right)\left(\frac{\boldsymbol{f}}{f_\mathrm{b}[k\boldsymbol{v}+\boldsymbol{c}]}\right). \tag{8}$$

A formal solution follows directly, by elementary manipulation. It is convenient to treat separately the case $k=0$ first: this has solution

$$\boldsymbol{f}_0 = \boldsymbol{A}^{-1}(\boldsymbol{v}_\mathrm{b} - f_\mathrm{b}\boldsymbol{B}\boldsymbol{c}) \tag{9}$$

and

$$\boldsymbol{v}_0 = \boldsymbol{C}\boldsymbol{A}^{-1}\boldsymbol{v}_\mathrm{b} + f_\mathrm{b}(\boldsymbol{D} - \boldsymbol{C}\boldsymbol{A}^{-1}\boldsymbol{B})\boldsymbol{c}. \tag{10}$$

Now the solution to the general case may be written

$$\boldsymbol{v} = [\boldsymbol{I} - f_\mathrm{b}k(\boldsymbol{D} - \boldsymbol{C}\boldsymbol{A}^{-1}\boldsymbol{B})]^{-1}\boldsymbol{v}_0 \tag{11}$$

and

$$\boldsymbol{f} = \boldsymbol{A}^{-1}[\boldsymbol{v}_\mathrm{b} - f_\mathrm{b}\boldsymbol{B}(k\boldsymbol{v}+\boldsymbol{c})]. \tag{12}$$

Note that the form of the matrix $\boldsymbol{A}$ guarantees that it is always non-singular, and at least for small enough values of $k$, the matrix in square brackets in eq. (11) is clearly non-singular since it is diagonal-dominant.

Essentially the same procedure may be applied to obtain formal solutions for a much wider class of periodic motions. One may choose a period, equal to the natural period or not, and go through one cycle designating each time step to be either sticking or slipping (provided there is at least one of each). The set of simultaneous equations corresponding to this choice may be written down, and by permuting rows and columns suitably, all the "sticking" equations may be collected before all the "slipping" ones. The result differs in form from eq. (7) only in the precise content of the matrix, but the procedure of partitioning and formal solution is not influenced at all, and a candidate periodic solution can be produced which corresponds to the chosen period, and sequence of sticking and slipping intervals. Thus we have potentially a very rich class of periodic solutions.

However, some of these may not satisfy the self-consistency conditions to make them true solutions to the problem as posed. We can list the required conditions as follows:

(a) no slipping velocity shall be greater than the limit for the assumed linear form in Fig. 1;
(b) no sticking force shall be higher than the maximum allowed for sticking friction;
(c) no sticking force shall be more negative than the limit of sticking friction in the reverse direction;
(d) any point which falls within the shaded region of Fig. 1 must obey the hysteresis rule, so that it must be in the same state (sticking or slipping) as the most recent preceding point which lies outside the shaded region.

Many of these conditions, when applied to a particular solution, can be cast in the form of limits on the allowed values of the normal bow force $f_\mathrm{b}$. The behaviour of the maximum and minimum bow forces for the Helmholtz motion has been discussed by various previous authors [3, 13, 14 §4.6], and similar discussions can be applied to the other possible periodic oscillation regimes. We return to this issue in Section 2.3. For now, we simply give one example of the type of solutions which arise from the procedure just outlined. We consider the case $p=3$, $q=4$, $f_\mathrm{b}=1$,

$k = 0.001$, $c = 0.3$, $\lambda = 0.99$, limiting coefficient of sticking friction equal to 0.8, and a maximum allowed velocity on the linear "slipping" segment of Fig. 1 equal to $0.8\,v_b$. Assuming the natural period of the string, there are 16 essentially different seven-sample periodic solutions, corresponding to the different possible sequences of sticking and slipping. For the parameters just specified, all 16 of these solutions satisfy the conditions (a)–(d) listed above, so they are all indeed solutions to the complete problem. The set of velocity waveforms is shown in Fig. 3, two cycles being plotted in each case.

## 2.2. Friedlanders' model as a limiting case

We next investigate limiting cases of Raman's model. There are two parameters in the problem which it is reasonable to regard as small: $k$ and $\varepsilon$. The limit in which both of these parameters tend to zero is not well behaved. In particular, quite different answers are found in the two cases in which one is set to zero, then the other allowed to tend to zero afterwards. It is sufficient to discuss the case represented in eq. (7), of a single-slip-per-cycle solution with the natural period of the string. The simpler of the two cases is that discussed by Friedlander. If we set $\varepsilon = 0$, then it is clear that the force must be constant throughout the cycle. If it were not, it would have fluctuations at resonant frequencies of the string, and with no mechanism of energy dissipation a steady state is not possible, since resonant growth of the string response must occur. However if force is constant during slipping and $k$ is non-zero, then the string velocity during slipping must also be constant, to be compatible with the relation (1) (provided $k \neq 0$). The constant value may be deduced from the fact that the velocity waveform must integrate to zero over one cycle in this model (although when $\varepsilon \neq 0$ it integrates to a non-zero value, which is small if $\varepsilon$ is small). The result remains unchanged throughout the limiting process $k \to 0$. For the case $r = p$, it is the ideal Helmholtz motion.

If instead we set $k = 0$ and then let $\varepsilon \to 0$, a very different picture is found. Note first the curious fact, proved in the Appendix, that the set of equations

$$\boldsymbol{M}\boldsymbol{x} = \mathbf{1} \tag{13}$$

has solutions $\boldsymbol{x}$ entirely in integers, where $\mathbf{1}$ is a vector of 1's and $\boldsymbol{M}$ is a symmetric matrix formed by deleting one or more rows and columns from the right and bottom of the matrix

$$\begin{pmatrix} 1 & -1/2 & & & -1/2 \\ & 1 & \ddots & -1/2 & \\ & & \ddots & \ddots & \ddots \\ -1/2 & & \ddots & \ddots & -1/2 \\ & \ddots & \ddots & & \\ -1/2 & & -1/2 & & 1 \end{pmatrix}$$

(where the pattern of non-zero elements matches the matrix of eq. (7)). This matrix has the form of the matrix $\boldsymbol{A}$ in the limit $\varepsilon \to 0$, apart from a factor $2/(1-\lambda^2)$. The matrix $\boldsymbol{C}$ in that limit contains only zeros and ones, multiplied by a factor $1/(1-\lambda^2)$ which cancels when the product $\boldsymbol{C}\boldsymbol{A}^{-1}$ is formed. It follows that the first term of the solution $\boldsymbol{v}_0$ from eq. (10) consists of integer multiples of $v_b/2$. The second term, involving $\boldsymbol{c}$, turns out on close inspection to be $O(\varepsilon)$, so that it does not contribute in the limit $\varepsilon \to 0$. Thus the waveform of velocity during slipping, for any solution in this class, consists quite unexpectedly of quantised values, in a mixture which adjusts to satisfy the condition that the integrated velocity over a cycle is zero. This is quite different from the constant slipping velocity given by taking the limits in the other order.

To see more clearly what is happening, we treat a particular example in detail. Consider the case $p = 3$,

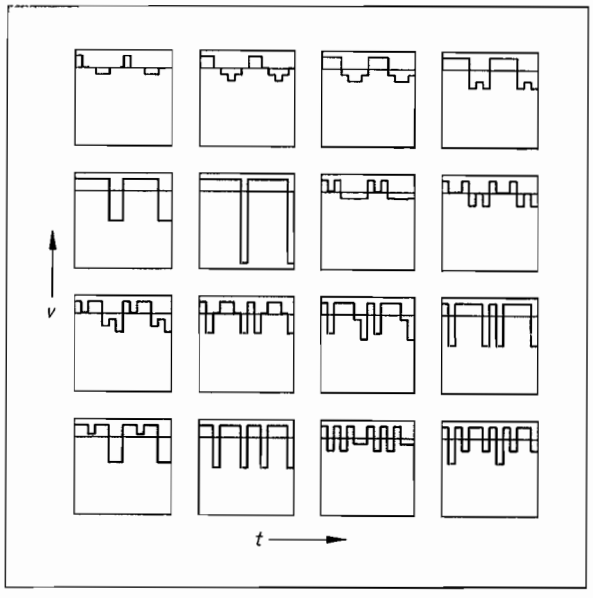


Fig. 3. The 16 different periodic solutions to Raman's model, using values $p = 3$, $q = 4$, $f_b = 1$, $v_b = 1$, $k = 0.001$, $c = 0.3$, $\lambda = 0.99$, coefficient of sticking friction 0.8, and maximum velocity on sliding portion of friction curve 0.8. Two cycles of velocity waveform are plotted in each case, and the vertical scale is the same throughout. The case at the top right is the "Helmholtz" solution for these parameter values.

$q = 4$, $r = 3$. The explicit form of the matrix of eq. (7) is

$$\frac{1}{1-\lambda^2}\begin{pmatrix} 1+\lambda^2 & 0 & 0 & -\lambda & -\lambda & 0 & 0 \\ 0 & 1+\lambda^2 & 0 & 0 & -\lambda & -\lambda & 0 \\ 0 & 0 & 1+\lambda^2 & 0 & 0 & -\lambda & -\lambda \\ -\lambda & 0 & 0 & 1+\lambda^2 & 0 & 0 & -\lambda \\ -\lambda & -\lambda & 0 & 0 & 1+\lambda^2 & 0 & 0 \\ 0 & -\lambda & -\lambda & 0 & 0 & 1+\lambda^2 & 0 \\ 0 & 0 & -\lambda & -\lambda & 0 & 0 & 1+\lambda^2 \end{pmatrix}.$$

Carrying through the manipulations yields the $k = 0$ solution

$$\boldsymbol{f}_0 = \begin{pmatrix} \dfrac{(1-\lambda^2)(1+\lambda+\lambda^2)}{1+\lambda^2+\lambda^4} v_b + \dfrac{\lambda(1+\lambda+\lambda^2)}{1+\lambda^2+\lambda^4} f_b c \\ \dfrac{(1-\lambda^2)}{1+\lambda^2} v_b + \dfrac{2\lambda}{1+\lambda^2} f_b c \\ \dfrac{(1-\lambda^2)}{1+\lambda^2} v_b + \dfrac{2\lambda}{1+\lambda^2} f_b c \\ \dfrac{(1-\lambda^2)(1+\lambda+\lambda^2)}{1+\lambda^2+\lambda^4} v_b + \dfrac{\lambda(1+\lambda+\lambda^2)}{1+\lambda^2+\lambda^4} f_b c \end{pmatrix} = \begin{pmatrix} f_b + 2\varepsilon v_b \\ f_b + \varepsilon v_b \\ f_b + \varepsilon v_b \\ f_b + 2\varepsilon v_b \end{pmatrix} + O(\varepsilon^2) \tag{14}$$

and

$$\boldsymbol{v}_0 = \begin{pmatrix} -\lambda\left[\dfrac{(1+\lambda+\lambda^2)}{1+\lambda^2+\lambda^4} + \dfrac{1}{1+\lambda^2}\right] v_b + \dfrac{(1+\lambda+\lambda^2)(1-\lambda^5)}{(1+\lambda)(1+\lambda^2)(1+\lambda^2+\lambda^4)} f_b c \\ -\dfrac{2\lambda}{1+\lambda^2} v_b + \dfrac{1-\lambda^2}{1+\lambda^2} f_b c \\ -\lambda\left[\dfrac{(1+\lambda+\lambda^2)}{1+\lambda^2+\lambda^4} + \dfrac{1}{1+\lambda^2}\right] v_b + \dfrac{(1+\lambda+\lambda^2)(1-\lambda^5)}{(1+\lambda)(1+\lambda^2)(1+\lambda^2+\lambda^4)} f_b c \end{pmatrix} = \begin{pmatrix} -\dfrac{3}{2} v_b + \dfrac{5}{4}\varepsilon f_b c \\ -v_b + \varepsilon f_b c \\ -\dfrac{3}{2} v_b + \dfrac{5}{4}\varepsilon f_b c \end{pmatrix} + O(\varepsilon^2). \tag{15}$$

The quantised form of the elements of $\boldsymbol{v}_0$ in the limit $\varepsilon \to 0$ is clear here, as are the facts that the force tends towards a constant value and the integral over a period of the velocity tends to zero in the same limit (recalling that there are four steps of sticking here, with velocity $v_b$).

To obtain the solution for finite $k$, we see from eq. (11) that the velocity vector is modified by the matrix $[\boldsymbol{I} - f_b k(\boldsymbol{D} - \boldsymbol{C}\boldsymbol{A}^{-1}\boldsymbol{B})]^{-1}$, which for this example is equal to

$$\begin{pmatrix} 1 - \dfrac{f_b k(1-\lambda^{10})}{(1-\lambda^4)(1-\lambda^6)} & \dfrac{f_b k \lambda^2}{(1-\lambda^4)} & \dfrac{f_b k \lambda^3}{(1-\lambda^6)} \\ \dfrac{f_b k \lambda^2}{(1-\lambda^4)} & 1 - \dfrac{f_b k(1+\lambda^4)}{(1-\lambda^4)} & \dfrac{f_b k \lambda^2}{(1-\lambda^4)} \\ \dfrac{f_b k \lambda^3}{(1-\lambda^6)} & \dfrac{f_b k \lambda^2}{(1-\lambda^4)} & 1 - \dfrac{f_b k(1-\lambda^{10})}{(1-\lambda^4)(1-\lambda^6)} \end{pmatrix}^{-1}$$

In the limit in which both $k$ and $\varepsilon$ are small, it is plain that this matrix depends to leading order only on the combination

$$\alpha = \frac{f_b k}{\varepsilon}, \tag{16}$$

involving the ratio of the two small quantities. It is the appearance of this ratio which accounts for the unexpected limiting behaviour noted above. The two cases discussed correspond to values of zero and infinity for $\alpha$, and we can now investigate what happens for intermediate values, at least for this particular example.

The approximate value of the matrix is (17)

$$\begin{pmatrix} 1-5\alpha/12 & \alpha/4 & \alpha/6 \\ \alpha/4 & 1-\alpha/2 & \alpha/4 \\ \alpha/6 & \alpha/4 & 1-5\alpha/12 \end{pmatrix}^{-1} = \frac{1}{1-3\alpha/4} \begin{pmatrix} \dfrac{1-11\alpha/12+7\alpha^2/48}{1-7\alpha/12} & -\alpha/4 & \dfrac{\alpha/6+7\alpha^2/48}{1-7\alpha/12} \\ -\alpha/4 & 1-\alpha/4 & -\alpha/4 \\ \dfrac{\alpha/6+7\alpha^2/48}{1-7\alpha/12} & -\alpha/4 & \dfrac{1-11\alpha/12+7\alpha^2/48}{1-7\alpha/12} \end{pmatrix}.$$

As $\alpha \to \infty$, it is easy to see that this matrix tends towards

$$\begin{pmatrix} 1/3 & 1/3 & 1/3 \\ 1/3 & 1/3 & 1/3 \\ 1/3 & 1/3 & 1/3 \end{pmatrix}$$

so that the vector $\boldsymbol{v}_0$ is simply averaged to produce the constant slipping velocity expected for that case (Friedlander's case).

To obtain an approximation to the general expression for $\boldsymbol{v}$, it is good enough to use the leading-order approximation $\boldsymbol{v}_0 \approx [-3v_b/2, -v_b, -3v_b/2]^t$ to obtain

$$\boldsymbol{v} \approx -\begin{pmatrix} \dfrac{\alpha-3/2}{3\alpha/4-1} \\ \dfrac{\alpha-1}{3\alpha/4-1} \\ \dfrac{\alpha-3/2}{3\alpha/4-1} \end{pmatrix} v_b. \tag{18}$$

This solution shows the expected behaviour for very large and very small $\alpha$, but the behaviour for intermediate values is by no means a simple interpolation between these two limits. Indeed, for a range of $\alpha$ around 4/3 the solution fails to satisfy one of the self-consistency conditions: one or other of the three slipping velocities exceeds the maximum allowed on the slipping portion of the friction curve. Thus not even the solution to the Raman model which approximates the Helmholtz motion can be guaranteed to satisfy all conditions of the problem, under (apparently quite realistic) conditions when $k$ and $\varepsilon$ are both small.

### 2.3. Bow force limits

The sensitivity of solutions just revealed, together with the unrealistic nature of starting transients seen in Fig. 2, are both good reasons for scepticism about the suitability of Raman's or Friedlander's model to explain observed phenomena in bowed strings. However, Raman showed that many of the periodic solutions to these models do correspond to regimes which have been observed [3, 15], so that provided caution is exercised the models can clarify aspects of the behaviour of these regimes. One area of enquiry in which Raman's model can contribute something useful is in the study of bow-force limits. The fact that any given note can only be produced with a bow force lying between certain limits is familiar to every violinist, and variations of the maximum and minimum bow forces between instruments, or between notes on one instrument, may contribute to the sense that some are "easier to play" than others [5, 6].

It is obviously of interest to know what governs these force limits, and how they are influenced by the various parameters of the problem. The best-known investigation of this issue is that of Schelleng [13], who summarised his results in a diagram of the force limits for the Helmholtz motion plotted against bow position on the string. (This position is usually specified by the fractional distance of the bow from the violin bridge, designated $\beta$ and equal to $p/(p+q)$ in terms of our treatment of Raman's model.) Of course, Raman's model contains by no means all the physical effects which might influence bow-force limits in practice, but nevertheless it is of interest to see what this model predicts for those limits since it is at present the only model which is understood well enough to give definite predictions without recourse to exhaustive simulation.

As was remarked earlier, the various self-consistency conditions which must be satisfied by a candidate periodic solution can be cast in the form of limits on bow force. By far the easiest case to study is that with $k = 0$, leading to eqs. (9) and (10). The dependence on $f_b$ is explicit in a very simple way here. In any case, this is the more relevant of the simple limits, in which $\alpha$ either goes to zero or infinity: it turns out that the requirement of stability sets an upper limit on $\alpha$ for each solution [11], with a value generally of the order of unity. (For the example analysed in detail in Section 2.2, the stability threshold is $\alpha = 4/3$.) Thus a requirement to be safely below this limit excludes most of the strong variation with $\alpha$, and the $\alpha = 0$ solution may be supposed to give a reasonable first approximation.

When all the conditions listed near the end of section 2.1 are turned into limits on bow force, it transpires that the maximum and minimum bow forces are almost invariably determined by the two conditions which Schelleng used. Minimum bow force occurs when the maximum of the force $\boldsymbol{f}$ during sticking just

exceeds the limit of friction, so that another slip must occur during the interval within which sticking was assumed in the analysis. Maximum bow force occurs when the left-hand boundary of the shaded region in Fig. 1 crosses the friction curve at the value of the first slipping velocity, $v_1$, so that a transition from sticking to slipping cannot occur at the assumed time (by the hysteresis rule stated earlier). It is a trivial matter to compute these force limits for any given solution, and we illustrate with some results for the family of single-slip-per-cycle solutions described by eq. (7). The results will all be presented in "Schelleng diagrams", for comparison with his work.

First, we show the behaviour of the "Helmholtz" solutions, having $r = p$. When results for all values $q \leqq 50$, $p < q$ are combined, the force limits map out the two curves plotted in Fig. 4. In broad terms, both limits follow the trend shown by Schelleng. He found (using a small-$\beta$ approximation) that minimum force varies as $\beta^{-2}$ while maximum force varies as $\beta^{-1}$, so that on the log-log plot they appear as straight lines with slopes $-2$ and $-1$ respectively. In detail, our results depart from such straight lines, and an obvious regularity in the behaviour is revealed: both limits form "staircases", in which the values remain constant in each interval $1/n > \beta > 1/(n+1)$ $(n = 2, 3, 4, \ldots)$. This constancy of value is exact to the precision of the computations, and probably reflects a result which could be explored analytically, but that possibility is pursued no further here. The end points of the ranges, where $\beta = 1/n$, behave differently for the two force limits. For the maximum bow force, the $1/n$ points give values intermediate between the constant values on either side, while for minimum force, the $1/n$ points agree with the constant value to the right of each point.

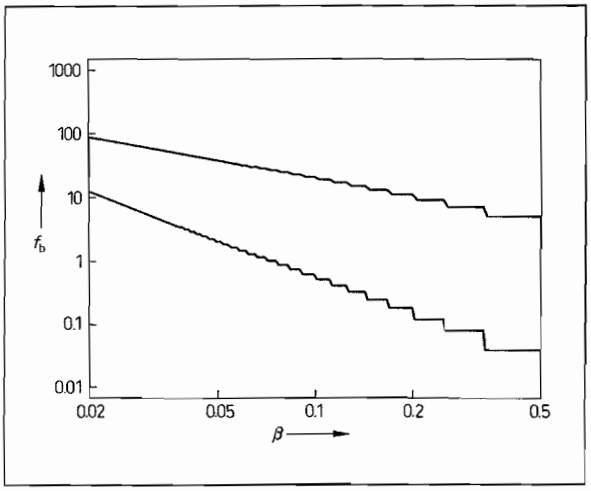


Fig. 4. Maximum and minimum bow force limits for the Helmholtz solution to the Raman model, plotted against $\beta$ on log-log axes in a "Schelleng diagram". Points are plotted for all values $q = 2, \ldots, 50$, $p = 1, \ldots, q-1$. Other parameters are: $v_b = 1$, $k = 0$, $c = 0.3$, $\lambda = 0.99$, coefficient of sticking friction 0.8, and maximum velocity on sliding portion of friction curve 0.8.

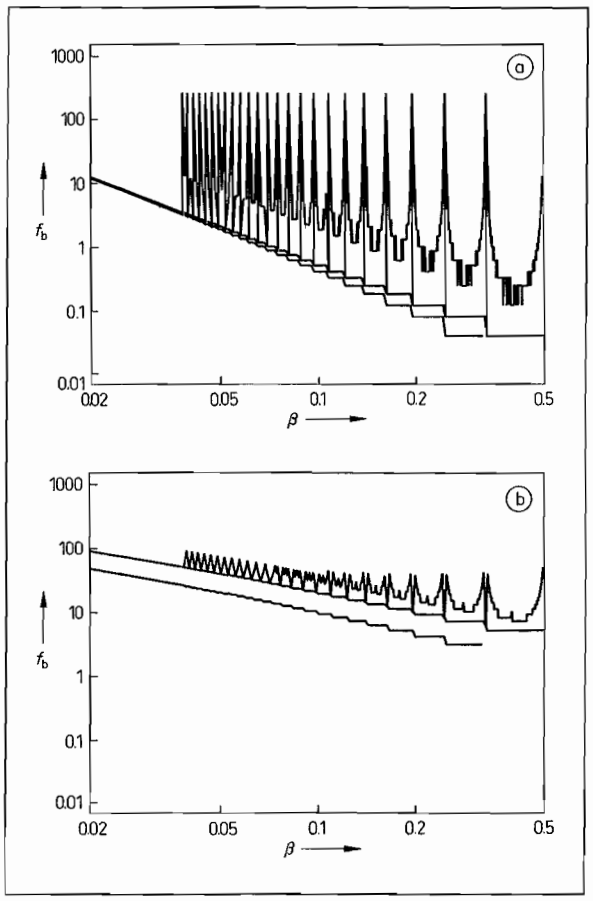


Fig. 5. a) Minimum bow force limits and b) maximum bow force limits plotted against $\beta$ for the same range of parameters as in Fig. 4, for three cases of slipping time $r$: lower curve $r = 2p$; middle curve $r = p$ (as in Fig. 4); upper curve $r =$ nearest integer above $p/2$. Scales are the same as in Fig. 4.

When the computations are carried out with values of $r$ different from $p$, quite different behaviour is found for the cases $r < p$ and $r > p$. It is hard to convey the behaviour for the full range of $r$, so we show two representative cases. Using the same range of $p$ and $q$ as above, solutions and force limits were calculated for $r$ equal to $2p$ and to the nearest integer above $p/2$. The three minimum force curves, including the one shown in Fig. 4, are plotted in Fig. 5a, and the three corresponding maximum force curves are plotted in Fig. 5b. Both force limits are found to increase monotonically as $r$ decreases, for all solutions, so that the $r = 2p$ curves appear lowest and the $r \approx p/2$ highest.

Again, striking regularities are revealed which might point towards interesting analytic results. The results for $r = 2p$ are generally similar to those for $r = p$, "staircases". In the case of minimum bow force, the values are all identical to those for $r = p$ except that each is shifted left into the next interval. The results for $r \approx p/2$ are quite different. Some kind of quantisation of values is still evident, but with a more complicated pattern. Both curves show an increase around each $1/n$ point, particularly strong in the case of minimum bow force. Note that for the cases with $p = 1$, the integer above $p/2$ is again 1, so that those points duplicate the $r = p$ results. For minimum force this produces vertical lines at $\beta = 1/n$, since the other points giving the same $\beta$ (2:2 $n$, 3:3 $n$ etc.) give a much higher answer. For maximum force, in contrast, all combinations giving the same $\beta$ give the same force limit, and notches appear in the curve around the $1/n$ points.

Finally, notice that for the $r \approx p/2$ curves, there is an interval of $\beta$ around each $1/n$ point for which the minimum force is higher than the maximum force. This means that the corresponding "solutions" are not self-consistent. Taking $r$ as an even smaller fraction of $p$ would make these regions wider. This may have relevance to a point raised recently by Weinreich and Caussé [16]: they point out that smaller values of $r$ may tend to be favoured on grounds of stability. This raises an obvious question of why, in practice, the Helmholtz motion is usually obtained in preference to some oscillation regime with a shorter slipping period. If such regimes are not in fact possible for a significant fraction of the possible values of $\beta$, as suggested by Fig. 5, it is perhaps not very surprising that they are rarely produced in practice.

## 3. Rounded-corner models

### 3.1. Integral equation and kernel functions

We now turn to consider a very different class of bowed-string models, from which the Raman and Friedlander models would be expected to appear as limiting cases. These models retain the assumption of point bowing and the friction-curve approximation, but allow a much more general class of (linear) behaviour to the string and its terminations. The theory has been developed in detail elsewhere [4, 5, 12]. The governing equation is now an integral equation

$$v(t) = \int_{-\infty}^{t} g(t-\tau) f(v(\tau))\,\mathrm{d}\tau \tag{19}$$

where $f(v)$ is the friction function, and $g(t)$ is the velocity response at the bowed point to a force impulse applied there. This impulse response function can be written in terms of the two reflection functions $h_1(t)$ and $h_2(t)$ which characterise the reflection behaviour of the sections of string to the left and right of the bowed point respectively [4, 5]:

$$g(t) = \frac{Y_0}{2}[\delta(t) + h_1(t) + h_2(t) + 2h_1 * h_2 + h_1 * h_2 * h_1 + h_2 * h_1 * h_2 + \ldots] \tag{20}$$

where * denotes the operation of convolution and $Y_0$ is the characteristic admittance of the string, as before. Again, it is convenient to choose units such that $Y_0 = 2$. If both reflection functions are unit delta functions, this becomes Friedlander's model, while if they are delta functions with amplitudes less than unity it is Raman's model.

We will seek periodic solutions to eq. (19). For a solution with period $T$, the range of integration in eq. (19) may be reduced to a single period

$$v(t) = \int_{0}^{T} k(t-\tau) f(v(\tau))\,\mathrm{d}\tau \tag{21}$$

where the kernel function $k(t)$ is a "folded-up" version of $g(t)$:

$$k(t) = \sum_{n=-\infty}^{\infty} g(t - nT), \quad (0 \leqq t \leqq T). \tag{22}$$

(Since $g(t)$ is a causal function, the terms corresponding to positive values of $n$ contribute nothing to $k(t)$, but this form is the most convenient.)

In the frequency domain, eq. (20) may be written

$$G(\omega) = \frac{1 + H_1 + H_2 + H_1 H_2}{1 - H_1 H_2} \tag{23}$$

where $G$, $H_1$ and $H_2$ denote the Fourier transforms of the corresponding functions denoted by lower-case letters [5]. To express eq. (22) in the frequency domain, we may take advantage of the Poisson summation formula:

$$\sum_{n=-\infty}^{\infty} g(t - nT) = \frac{1}{T} \sum_{n=-\infty}^{\infty} G\left(\frac{2\pi n}{T}\right) \exp\left(\frac{2\pi i n t}{T}\right) \tag{24}$$

so that the Fourier series coefficients of $k(t)$ are simply values of $G(\omega)$ sampled at $\omega = 2\pi n/T$.

We will concentrate on the particular case in which both reflection functions are significantly non-zero only for a time interval short compared with the period of the motion. Aspects of the behaviour of such "narrow reflection functions" have been discussed previously [5, 6]. The aim here is to investigate the limit in which the widths of both functions tend to zero, to see whether the solutions then approach those of the Raman model discussed earlier. The first stage is to examine the behaviour of the kernel function $k(t)$ in

this limit. Narrowness of the reflection functions corresponds to slow variation of the appropriate sampled values of $G$ at low values of $n$. We may thus find leading-order approximations for the Fourier coefficients of $k(t)$ by expanding $H_1(\omega)$ and $H_2(\omega)$ as Taylor series, then using eqs. (23) and (24).

It turns out that we need expansions correct to $O(\omega^2)$ to deal with the various cases of interest. Define quantities $\lambda_1$, $t_1$ and $\Delta_1$, following notation used earlier and in reference [5], via

$$\lambda_1 = -\int_{-\infty}^{\infty} h_1(t)\,dt, \tag{25}$$

$$\int_{-\infty}^{\infty} (t - t_1) h_1(t)\,dt = 0 \tag{26}$$

and

$$2\Delta_1^2 = -\int_{-\infty}^{\infty} (t - t_1)^2 h_1(t)\,dt. \tag{27}$$

Corresponding quantities $\lambda_2$, $t_2$ and $\Delta_2$ are similarly defined from $h_2(t)$. Now it is readily shown that

$$H_1(\omega) = -\lambda_1 \exp(-i\omega t_1) + \omega^2 \Delta_1^2 + O(\omega^3), \tag{28}$$

with a corresponding expression for $H_2(\omega)$. Substituting into eq. (23) thus yields

$$G(\omega) \approx \frac{1 - \lambda_1 \exp(-i\omega t_1) - \lambda_2 \exp(-i\omega t_2) + \lambda_1 \lambda_1 \exp(-i\omega(t_1 + t_2)) + \omega^2 [\Delta_1^2 (1 - \lambda_2) + \Delta_2^2 (1 - \lambda_1)]}{1 - \lambda_1 \lambda_1 \exp(-i\omega(t_1 + t_2)) + \omega^2 [\lambda_2 \Delta_1^2 + \lambda_1 \Delta_2^2]}. \tag{29}$$

Three different cases of the behaviour of this expression may be distinguished, depending on the values of the various parameters. We are interested in the sampled values

$$k_n = G\left(\frac{2\pi n}{T}\right) \tag{30}$$

where the period $T$ might be the "natural" period $t_1 + t_2$ [5] or something different. For the Raman-model case with $\Delta_1 = 0$, $\Delta_2 = 0$ and using the natural period, we obtain

$$k_n \approx \frac{1}{1 - \lambda_1 \lambda_2} \{1 + \lambda_1 \lambda_2 - \lambda_1 \cdot \exp(-2\pi i n t_1/T) - \lambda_2 \exp(-2\pi i n t_2/T)\}. \tag{31}$$

This expression is in fact exact for this particular case. Using eqs. (22) and (24), it gives a kernel function $k(t)$ consisting of three delta functions, as illustrated in Fig. 6a. Eq. (21) then corresponds directly to eq. (5), for the case in which both $f_n$ and $v_n$ are periodic with period $N$.

For the rounded-corner case with the natural period and satisfying the constraint $\lambda_1 = \lambda_2 = 1$, eq. (29) gives

$$k_n \approx \frac{2 - \exp(-2\pi i n t_1/T) - \exp(-2\pi i n t_2/T)}{(2\pi n/T)^2 (\Delta_1^2 + \Delta_2^2)} \tag{32}$$

to leading order. This expression is valid for values of $n$ such that $(2\pi n/T)^2 (\Delta_1^2 + \Delta_2^2) \ll 1$. If it is used for all $n$, it is easy to see that it leads to a kernel $k(t)$ whose shape is the second integral of that of Fig. 6a, plotted in Fig. 6b. The Fourier series converges rapidly, so this piecewise-linear kernel will give an approximation to the true one except for two factors. First, at $t = 0$ the impulse response function (2) has a delta function contribution, which must of course appear in $k(t)$. Second, and probably less important, if the reflection functions are smooth, then $k(t)$ cannot actually have slope discontinuities at the points $T\beta$, $T(1 - \beta)$ as plotted in Fig. 6b, and on a small scale the corners can be no sharper than the functions $h_1(t)$, $h_2(t)$.

This "bucket-shaped" kernel, with the initial delta function restored, offers some hope of being a canonical case for periodic motion with the natural period of the string and narrow reflection functions: the detailed shapes of the reflection functions do not affect it, so that solutions obtained using it might apply to all models within the class. It is interesting that no rounding as such appears in the expression: the finite widths of the reflection functions appear only via an overall scaling factor. As the widths of the reflection functions tend to zero, we certainly do not obtain the same answer as the limit of the Raman-model kernel of Fig. 6a as $\lambda_1, \lambda_2 \to 1$. Both kernels show behaviour in which a scale factor tends to infinity, but the shapes which are scaled are very different. There is no obvious reason, then, to expect the solutions to be the same in that limit.

Before examining such solutions, we consider one more limiting case of eq. (29). So far, we have used only the natural period of the string, but, as has been explained previously [12], when we allow for hysteresis in the friction curve the Helmholtz motion, and other periodic regimes, exhibit periods somewhat longer than this (the "flattening effect"). It is thus of interest to see what happens to the kernel function when the period differs slightly from $t_1 + t_2$. If the period is lengthened by a factor $(1 + \eta)$, then to leading order

$$k_n \approx \frac{2 - \exp(-2\pi i n t_1/T) - \exp(-2\pi i n t_2/T)}{2\pi i n \eta} \tag{33}$$

where we retain the assumption $\lambda_1 = \lambda_2 = 1$. This is valid provided $(2\pi n/T)^2 (\Delta_1^2 + \Delta_2^2) \ll |2\pi n \eta| \ll 1$. Again, it is easy to see the kernel shape which arises if we apply this result for all $n$: it is the intermediate case between Figs. 6a and b, plotted in Fig. 6c for positive

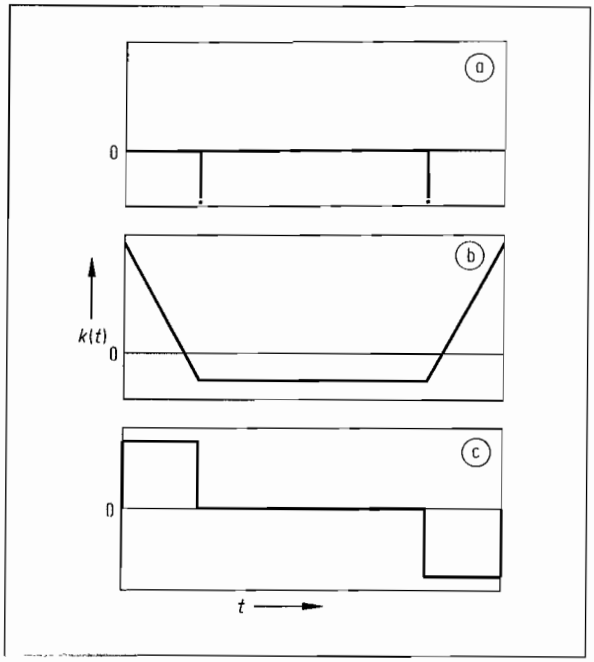


Fig. 6. Sketches of the three idealised kernel shapes $k(t)$ discussed in the text: a) Raman's model; b) the "bucket" kernel, arising from narrow reflection functions at the natural period; c) kernel arising from narrow reflection functions with a period longer than the natural period (for a shorter period, the picture is inverted).

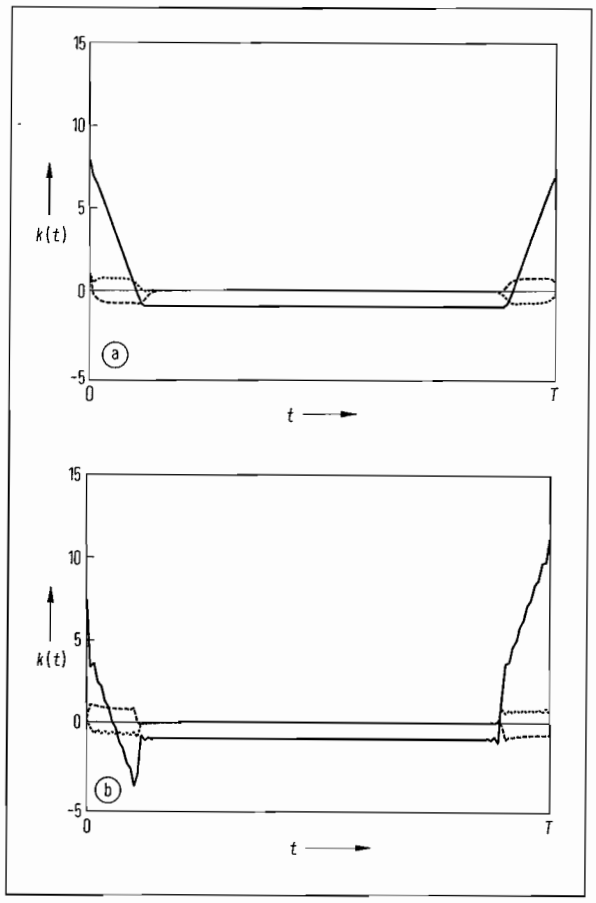


Fig. 7. Kernel functions $k(t)$ calculated for $\beta = 0.11$ a) with reflection functions which are identical Gaussian functions (apart from the different time delays), having a width such that the second moment matches that for Cremer's model; and b) from Cremer's model. In both cases, the solid curve corresponds to the natural period of the system, the dotted curve to a period 1% longer, and the dashed curve to a period 1% shorter. The vertical scale shows values in discretised form corresponding to 128 time steps per period.

$\eta$ (it is inverted for negative $\eta$). This time the overall scale factor contains $\eta$, so that as the pitch shift increases the amplitude of the kernel becomes smaller. The same remarks apply to this kernel as to that of Fig. 6b: it will be inaccurate near the sharp corners, and it lacks the initial delta function, but otherwise it is a candidate for the canonical problem for the class of periodic motions with narrow reflection functions and frictional hysteresis.

It is of interest to compare the approximate kernel shapes of Fig. 6 with examples calculated from specific models with narrow reflection functions. The closest match is obtained if we take a model with time-symmetric reflection functions. Such models are not physically realistic, but they make a useful test case for studying such effects as flattening due to frictional hysteresis [12]. Fig. 7a shows three kernels corresponding to a model with identical Gaussian functions for the two reflections, using the natural period, and periods 1% less and 1% greater. The shapes correspond very obviously to those of Fig. 6b and c. The kernels were calculated using a 128-point fast Fourier transform, and the vertical axis scale shows values corresponding to integration of the function over each of the 128 discrete time intervals making up a period: this is done in preparation for solution of the discretised version of the problem in the next section. Notice that this integration makes the unit delta function at $t = 0$ appear as an elevation of the first point by unity above the smooth underlying functions.

When kernels are calculated from other models, the shapes may not agree quite so well with the approximate ones. A particular case of some interest is Cremer's model [14, § 5.4], in which an ideal text-book string is terminated in a "body" model consisting of a spring and dashpot in parallel, with parameter values chosen to match approximately the frequency-dependent decay rates of overtones on a particular violin A-string. This model has been discussed elsewhere as an example of narrow reflection functions [5]. It has a delta-function reflection from one end of the string, which is assumed rigidly anchored, while the reflection

from the "body" is described by a delta function followed by an exponential "tail" as the spring-dashpot combination recovers its equilibrium position. When kernels are calculated for this model using the "correct" period, and periods 1% longer and 1% shorter, the results are as shown in Fig. 7b. The two perturbed periods both produce kernels bearing an obvious resemblance to Fig. 6c, while the natural period in this case produces a kernel which is recognisably related to Fig. 6b, albeit a little distorted. The width of the Gaussian reflection functions in Fig. 6a was chosen to give the same second moment as that for the "body" reflection function of Cremer's model, so that the two cases are immediately comparable.

### 3.2. Solutions with the idealised kernels

It is not easy to make progress finding analytic solutions for periodic motion using kernels other than the Raman-model one, but if we retain the piecewise-linear friction model used in Section 2 it is straightforward to compute examples. Numerical solutions using the integral eq. (21) have been presented by Schumacher [17], using a similar approach to that employed here, but it is worth giving some examples here since examination of them reveals interesting points of similarity and contrast with the discussion in Section 2. We will consider some cases of periodic solutions using the "bucket" kernel shown in Fig. 6b, which was argued to be a canonical problem for any model with narrow reflection functions, for oscillation with the natural period.

First, it is important to see why the delta function at $t = 0$ must be included in the kernel. It is clear from Fig. 1 that $f(t)$ and $v(t)$ must have jumps at the transitions between sticking and slipping in order to be compatible with the assumed friction law. However we know that $f(t)$ must be bounded (by the limits of friction for a given normal force), so that if $k(t)$ is a continuous function, then by eq. (21) $v(t)$ would be continuous. This contradiction may be resolved by including the initial delta function. Write

$$k(t) = \delta(t) + \tilde{k}(t), \tag{34}$$

where $\tilde{k}(t)$ will be continuous if both reflection functions from which it is derived are smooth, and will be assumed here to have the piecewise-linear "bucket" form (with integrated value $-1$ to allow for the removal of the unit delta function). Then eq. (21) becomes

$$v(t) = f(t) + \int_0^T \tilde{k}(t-\tau)\, f(v(\tau))\, \mathrm{d}\tau . \tag{35}$$

Now $v - f$ will be continuous by the previous argument, but $v$ and $f$ separately can have the required jumps (of equal magnitude).

The simplest procedure for obtaining numerical solutions is virtually the same as was described in Section 2.1. We first discretise the waveforms $v(t)$ and $f(t)$ at some chosen temporal resolution. If we now assume a single-slip-per-cycle solution and the same piecewise-linear friction curve as before, then the formal problem is identical to that of eq. (7) except that the matrix contains different entries. This matrix multiplying the vector of forces represents the convolution integral of eq. (21) in discrete form, so the matrix is now replaced with a circulant matrix whose first row is the appropriate discretised form of $k(t)$. The procedure of eqs. (8)–(12) now yields a formal solution, which must be checked against the same set of self-consistency conditions listed earlier. As with the Raman model discussed earlier, the procedure can be readily generalised to solutions with more than one slip per cycle, by rearranging the rows and columns of the matrix before partitioning and solving.

To illustrate the procedure, and explore the similarities to and differences from the Raman-model results described earlier, it is sufficient to consider only cases with a single episode of slipping in each cycle. To facilitate direct comparison we may take $\beta = 3/7$ as before, but to allow for the resolution of more rounded waveforms we now divide each cycle into 70 time steps. We use the "bucket" kernel suitably discretised into this number of points, with an amplitude which is approximately half that determined by the reflection functions of Cremer's model with this time discretisation and value of $\beta$. This corresponds to reflection functions which are a little broader than that of Cremer's model, so that velocity waveforms will be expected to be rather more smoothly-varying. The values in the first row of the circulant matrix plotted are in Fig. 8.

First, we show some results calculated by the procedure described above, when the slope of the slipping friction curve, $k$, is zero. These are plotted in Fig. 9 for a range of assumed sticking times, in multiples of 10 time steps from 10 to 60. The nominal Helmholtz motion for this case would stick for 40 time steps per period. In each case, one cycle of $v(t)$ is shown as a solid line while $v(t) - f(t)$ is shown as a dashed line. The velocity waveforms show smooth variation during slipping, in obvious contrast with the discontinuous solutions to the Raman model shown in Fig. 3.

The next step is to check the self-consistency conditions to see which (if any) of the computed results satisfy the full specification of the problem. In the case of the Raman model, this led to limits on the allowed value of bow force. The results of applying those conditions to the present calculations is quite different. Recall that we are expecting $v - f$ to approximate a discretely-sampled continuous function, while $v$ will

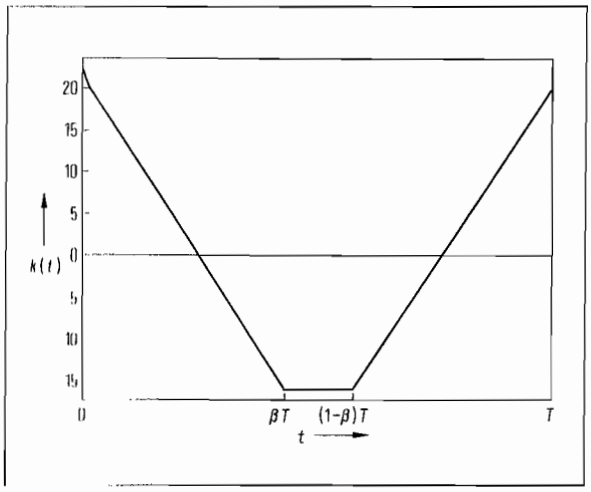


Fig. 8. Kernel function, in appropriate discretised form for 70 time steps per period, used in the computed examples. It is the "bucket" kernel, with the initial delta-function restored, for $\beta = 3/7$.

genuinely have jumps at the transitions between sticking and slipping. (This distinction cannot, of course, be seen clearly in any solution based on a particular discretisation, but it can be confirmed by varying the length of assumed time step.) For a given friction function, there is a critical value of $v - f$ which divides the sticking state from the slipping state. All the self-consistency conditions can be included in the statement that $v - f$ must pass through this value at the moments of transition between sticking and slipping, and not cross it at any other times. Note that frictional hysteresis does not enter this particular problem, because we are using the time-symmetric kernel appropriate to self-excited oscillation at the natural period of the free string. All the velocity waveforms shown in Fig. 9 are time-symmetric, whereas the flattening produced by frictional hysteresis is associated with a lack of symmetry between the transitions from sticking to slipping and vice versa [12]. The equivalent canonical problem with hysteresis would involve the "staircase" kernel of Fig. 6c, but that possibility is not pursued here.

A procedure to find allowed solutions is thus as follows. The waveforms are computed for all possible lengths of sticking time per cycle. The critical value of $v - f$ for the desired friction curve must be bracketed by the computed values for the last sticking point and the first slipping point, and no consecutive pair of values during either the sticking phase or the slipping phase must cross the critical value. For the case illustrated here, the second condition is readily satisfied, since it turns out that for every case the first and last sticking values of $v - f$ are smaller than all other sticking values, while the first and last slipping values are greater than all the others.

A graphical approach can now be used. In Fig. 10 the values of $v - f$ before and after the transition are plotted against length of sticking interval. The critical value for a given friction function can be shown as a horizontal line: two examples are shown on the figure, corresponding to the two friction functions shown in Fig. 11. Within the level of discretisation of these computed waveforms, any cases for which the horizontal line lies within the band delimited by the two curves qualify as possible periodic solutions to the problem; but the "correct" solutions are presumably much more tightly defined than this: we expect the true $v - f$ to be continuous, so that repeating the calculation with a shorter time step will make the band of allowed values narrower. The best guess based on the results shown here might be that solutions occur where the horizontal line corresponding to the chosen friction function intersects a curve lying mid-way between the two limits plotted.

This behaviour contrasts with that of Raman's model, discussed earlier. In that case, $v - f$ generally had finite jumps between successive points. Thus the critical value could be leapfrogged, as indeed could be a finite range within which hysteresis would otherwise have operated. The self-consistency conditions simply had to ensure that the jumps encompassed the range required, and this produced the finite ranges of allowed normal force illustrated, for example, in Figs. 4 and 5.

It is a shortcoming of the particular combination of friction model and kernel used here that it is not possible to treat variations in bow force consistently. Suppose, for example, that in the case plotted in Fig. 11a the bow force were increased, thus scaling the whole curve up by some constant factor. This would produce a range of $v - f$ over which hysteresis would occur, which is incompatible with the kernel function in use here. On the other hand, if the bow force were decreased there would be a range of $v - f$ in which the line of slope unity (see Fig. 1) would not intersect either desired branch of the friction relation, again violating the assumptions made in the calculation. Nevertheless the simplicity of the model used here makes it sensible to extract as much insight into the behaviour of the solutions as we may.

Examination of the two friction functions plotted in Fig. 11 shows that the difference between them is at least similar to that produced by a change in normal force. In particular, the jump in force between the limit of sticking friction and value for sliding friction is increased. The value of sliding friction force is unchanged, but this is immaterial: the mean value of the friction force plays no role since the kernel function

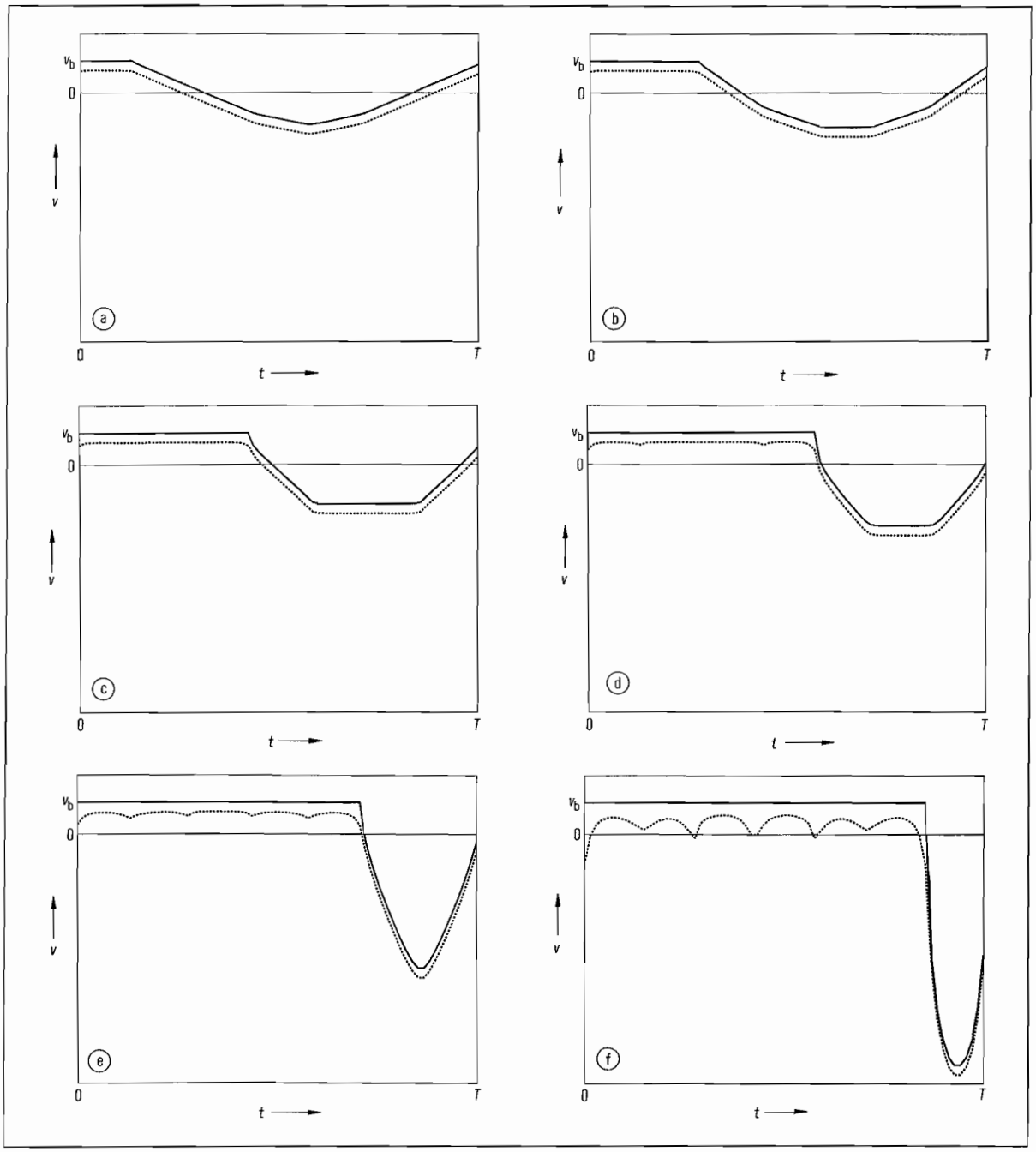


Fig. 9. Computed periodic solutions using the kernel of Fig. 8 and $k = 0$, with assumed slip times a) 60, b) 50, c) 40, d) 30, e) 20 and f) 10 time steps. Other parameters are: $f_b = 1$, $v_b = 1$, $c = 0.3$. The solid curves show $v(t)$, the dashed curve $v(t) - f(t)$. One period is shown in each case, and the vertical scale is the same throughout.

integrates to zero over a complete period. If we make this tentative identification that a lower horizontal line in Fig. 10 is rather like a higher bow force, then the falling shape of the curves in Fig. 10 produces a prediction which is consistent with other studies [12, 14, § 5.5]: when the bow force is decreased for a given oscillation regime, the length of slipping interval increases. In other terms, lower bow force results in a travelling Helmholtz corner which is less sharp.

There is another feature of the curves in Fig. 10 which deserves comment. They seem to be made up of several separate curve segments with transitions near the values of sticking interval 30, 40, 50 and 60. These presumably correspond to different regimes of oscilla-

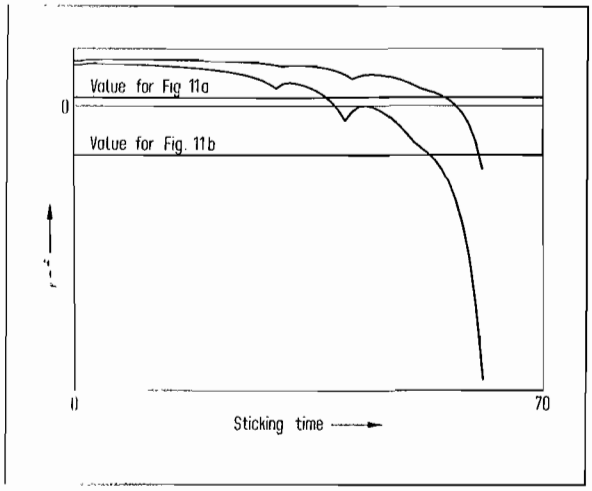


Fig. 10. Bow force limits, for single-slip-per-cycle periodic solutions to the rounded-corner model as in Fig. 9. The construction to find the "best" slip time is described in the text.

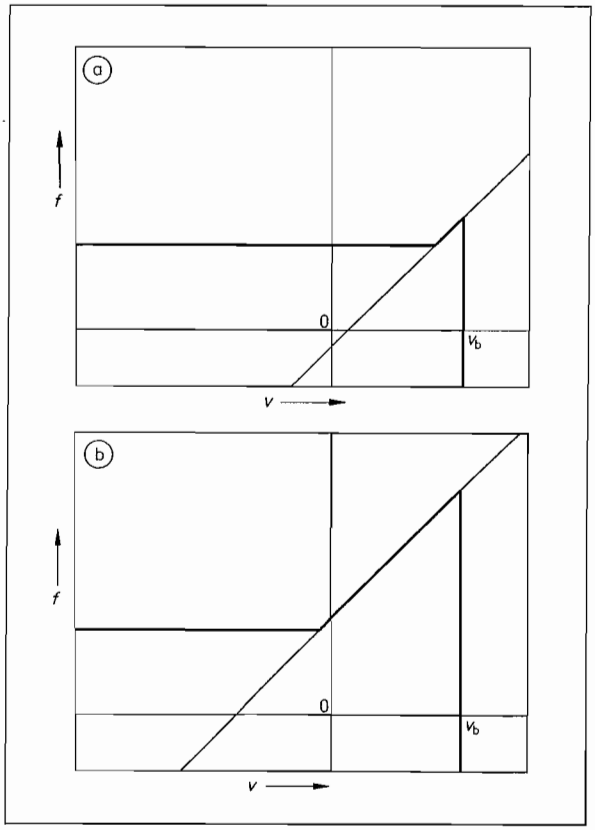


Fig. 11. Two cases of piecewise-linear friction curves with $k = 0$ and no hysteresis, as described in the text.

tion of the string, approximating to different members of Raman's classification into "higher types" [3]. (Note that the short rising portions of the curves near some of these transitions may be an artefact of plotting, since successive values are simply joined by line segments. When there is a change of regime, there might well be a sharp jump in the curves.) Thus this simple model, with all its shortcomings, may be able to shed a little light on the long-standing problem, alluded to in section 2, of how to tell which of the rich array of possible periodic solutions to Raman's model will survive in a model with reflection functions of finite width. This question undoubtedly merits further study, but is not pursued here.

Next, we examine what happens to the solutions when the slope $k$ of the slipping-friction curve is made non-zero. This is illustrated by the "Helmholtz" case of the family studied above, sticking for 40 time steps per period of 70 time steps. A sequence of waveforms of $v(t)$ is shown in Fig. 12. When $k = 0$ we have the solution already seen. As $k$ increases, the shape changes gradually, until the "solution" begins to require a slipping speed greater than the bow speed, which violates the model assumptions. This shape changes through an alternative form (Fig. 12d) as $k$ becomes even larger. This sequence of shapes is somewhat similar to that calculated from the Raman model, given in eq. (18). This strongly suggests that some aspects of the strange limiting behaviour of Raman's model, explored in Section 2, carries over to models with reflection functions with finite width.

It is possible that there is some physical significance in these last results: the waveform shown in Fig. 12d suggests that the "Helmholtz" motion might give way to an oscillation regime in which there are two short slipping phases with a short sticking phase in between, under conditions when the friction curve slope is high. This might bear upon the formation of "multiple-fly-back" regimes, discussed elsewhere [6, 18], which are sometimes favoured over the Helmholtz motion in a starting transient in which the bow force is initially high. Such regimes have been found in simulation studies using models with narrow reflection functions, and have also been observed on real violin strings.

### 3.3. The Friedlander limit of rounded-corner models

The final issue to be examined concerns the limiting form of the solutions when the model is allowed to tend towards the "Friedlander" case. We have already seen that the kernel $k(t)$ does not tend towards the delta-function Friedlander/Raman kernel. However many solutions to Raman's model are known to give a good first approximation to what is found in reality, so presumably the solutions to the models in this limit are more similar than simple examination of the kernel functions might suggest.

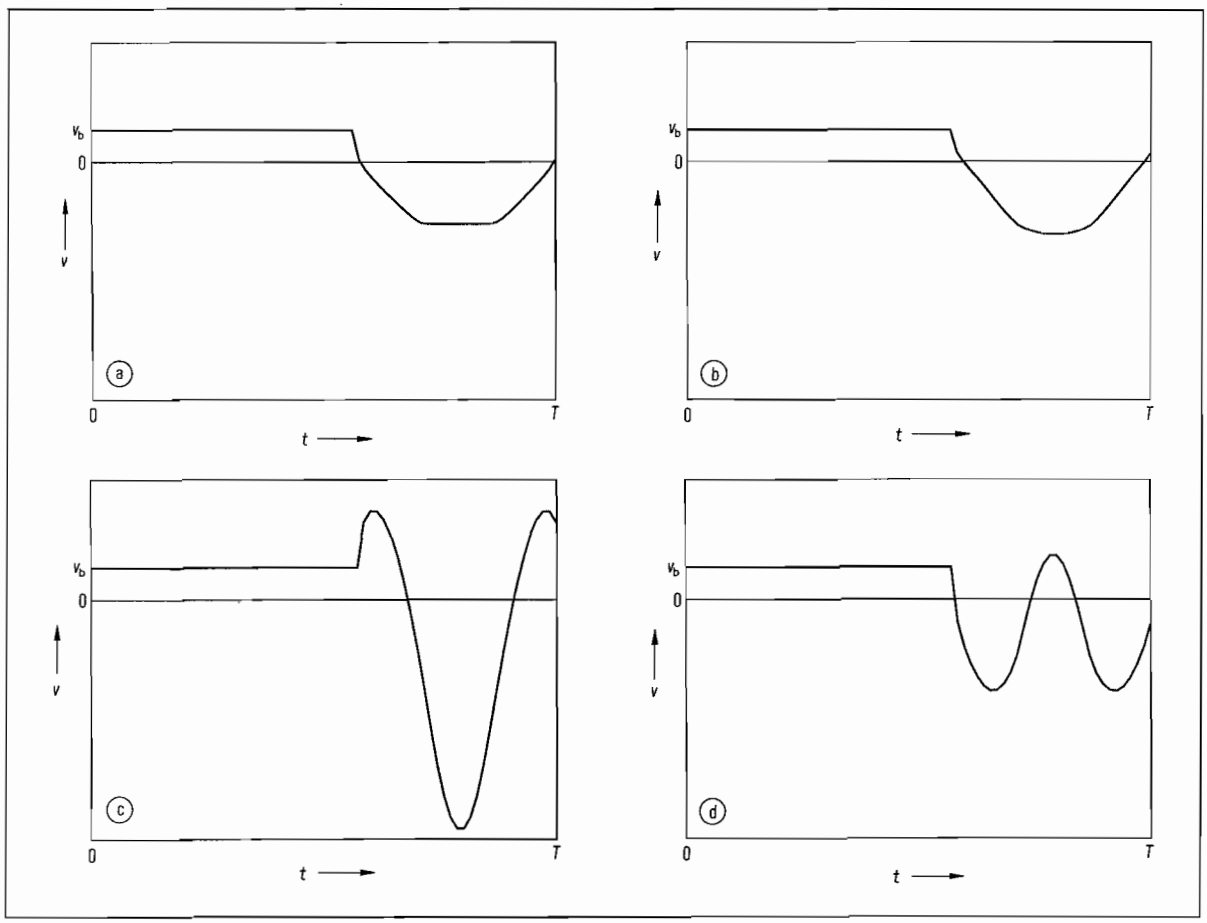


Fig. 12. The influence of friction-curve slope $k$ on periodic solutions to the rounded-corner model. Parameters are as for Fig. 9, but with a) $k = 0$; b) $k = 0.01$; c) $k = 0.03$; d) $k = 0.05$.

To obtain some insight into this question by analytic means, it is convenient to take a different approach to the solution of eq. (21). It will be recalled from Section 3.1 that the width of the reflection functions manifests itself in the "bucket" kernel only through an overall scale factor – narrower functions make the kernel bigger, and in the Friedlander limit of unit delta-function reflections the scale factor tends to infinity. This is the limit we wish to consider, but it is not easy to follow the consequences of scaling $k(t)$ through the matrix partitioning procedure presented above. This is the only procedure which allows us to solve for a mixture of unknown forces (during sticking) and unknown velocities (during slipping), which is necessary to treat the general case. However, if we restrict attention to the case $k \neq 0$, it is possible to solve instead for the force waveform $f(t)$ over the entire period, since the velocity during slipping can be uniquely recovered from it using the assumed friction relation (1).

First, $k(t)$ and $f(t)$ may be expressed in terms of Fourier series:

$$k(t) = \sum_n k_n \exp(2\pi i n/T) \tag{36}$$

and

$$f(t) = \sum_n f_n \exp(2\pi i n/T). \tag{37}$$

Now assume a solution with a single episode of slipping per cycle, of duration $\varrho T$ (where $\varrho = \beta$ for the ideal Helmholtz motion). The general problem (21) may then be written

$$T \sum_n k_n f_n \exp(2\pi i n t/T) = \begin{cases} v_b & (0 \leqq t \leqq \varrho T) \\ [f/f_b - c]/k & (\varrho T \leqq t \leqq T) \end{cases} \tag{38}$$

(using the convolution theorem for Fourier series). Multiplying by $\exp(-2\pi i m t/T)$ and integrating

over one period then yields

$$T k_m f_m = \left(v_b + \frac{c}{k}\right)\frac{[1 - \exp(-2\pi i m \varrho)]}{2\pi i m} + \frac{1}{k f_b}\sum_n f_n \frac{[1 - \exp(2\pi i (n-m)\varrho)]}{2\pi i (n-m)}. \quad (39)$$

So far as the unknown Fourier coefficients $f_m$ are concerned, this is a set of linear simultaneous equations. Presumably a possible solution procedure would be to truncate the set, choosing a suitable truncation order by a convergence test, but this is rather cumbersome, and does not compete in efficiency with the procedure used earlier, which in any case dealt with the more general case in which the value of $k$ was unrestricted.

The advantage of this approach is that it reveals very easily what happens in the Friedlander limit. If any one of the coefficients $k_m$ is allowed to tend to infinity, it is clear that the corresponding value $f_m$ must tend to zero to keep the product on the left-hand side of eq. (39) finite. This argument will in general apply to all the Fourier components except for $m = 0$. Reflection functions satisfying $\lambda_1 = \lambda_2 = 1$ (see eq. (25)) will have $k_0 = 0$, so that $f(t)$ can have a non-zero mean value as we expect, but if none of the other Fourier coefficients of the kernel vanish, then in the Friedlander limit all other Fourier coefficients of $f(t)$ will tend to zero. So $f(t)$ tends towards a constant value. It follows that the velocity can only take two values, $v_b$ during sticking and a constant value during slipping which is governed by the fact that $v(t)$ must integrate to zero over one cycle. In other words, any kernel function whatever, when multiplied by a scale factor which is allowed to tend to infinity, will give periodic solutions matching those of the Friedlander model (including the ideal Helmholtz motion). This argument only breaks down if the kernel function has any missing harmonics in its Fourier series, but this generally arises only when the bowed point falls exactly at a node of a vibration mode of the coupled string/body system, in which case that mode cannot be driven by the applied force from the bow and the corresponding Fourier coefficient of $v(t)$ will be zero.

This limit can be explored using examples computed by the method described in the previous subsection. As the scale factor is increased, a sequence of events is observed which initially follows that of Fig. 12. As the scale factor is increased further, the undesirable "wiggles" in the velocity waveform become progressively higher in frequency, but then with a further increase in scale factor this behaviour gives way once more to smooth variation of velocity during slipping, which does indeed tend towards a constant value, as predicted by the argument above.

## 4. Conclusions

Various idealised models for the self-excited motion of a bowed string have been studied, particularly in relation to possible periodic solutions. Friedlander's model, with no boundary losses and perfect delta-function reflections, has been considered as a limit of Raman's model (with delta-function reflections involving some energy loss) and of rounded-corner models in which the reflection functions are narrow compared with the period of the motion. In both cases, the limiting process was not straightforward, and the set of periodic solutions of the Friedlander model do not give a good guide to solutions of the other models.

Procedures have been given for finding all possible periodic solutions to the various models considered. In a companion paper [11], corresponding procedures for investigating the stability of these solutions are described. Examples have been given of the behaviour of the various models, but there is no doubt that more detail remains to be discovered. Future investigations could couple the methods used here with the use of systematic simulation described elsewhere [6], in an effort to shed more light on the question of which features of the modelling of the violin string and body might contribute to subjective impressions of "ease of playing".

## Acknowledgements

The author is extremely indebted to Dr. D. J. Allwright for the analysis given in the Appendix. Several colleagues have contributed to valuable discussions on this work, especially Dr. M. E. McIntyre and Professor R. T. Schumacher.

## Appendix

The matrix $\boldsymbol{M}$ in eq. (13), with no rows or columns deleted, is square with dimension $N$. So the $i$'th of eqs. (13) with no deletions may be written

$$x_i = 1 + [x_{i-p} + x_{i+p}]/2 \quad (A1)$$

where the subscripts are all to be taken as integers mod $N$. Now let $D$ be the set of indices of the deleted rows and columns. Then eq. (A1) holds for $i$ not in $D$, but for $i$ in $D$ it is replaced by

$$x_i = 0. \quad (A2)$$

The solution may be written in the form

$$x_i = (\text{least } j \text{ such that } i + jp \,(\text{mod } N) \text{ is in } D) \times (\text{least } k \text{ such that } i - kp \,(\text{mod } N) \text{ is in } D) \quad (A3)$$

where $j$ and $k$ are non-negative integers, so that $x_i$ is always an integer. Eq. (A 2) is obviously satisfied by this since $j$ and $k$ are both zero when $i$ is in $D$, and eq. (A 1) is also satisfied by virtue of the identity

$$jk = 1 + [(j+1)(k-1) + (j-1)(k+1)]/2. \qquad \text{(A 4)}$$

Note that $x_i$ is finite only if $D$ can be reached from $i$ by steps of $p \pmod N$, i.e. only if $i$ is congruent to some element of $D \pmod h$, where $h = \mathrm{HCF}(p, N)$. Since we assumed in the beginning that $p$ and $N$ were co-prime, this is always satisfied. Otherwise, $D$ would have to contain at least one index from each residue class $(\mathrm{mod}\ h)$, so that if $D$ consisted of a consecutive set of columns then it would need to contain at least $h$ columns.

## References


[1] Friedlander, F. G., On the oscillations of a bowed string. Proc. Cambridge Philos. Soc. **49** [1953], 516–530.

[2] Keller, J. B., Bowing of violin strings. Comm. Pure Appl. Math. **6** [1953], 483–495.

[3] Raman, C. V., On the mechanical theory of vibrations of bowed strings. Indian Assoc. Cult. Sci. Bull. **15** [1918], 1–158.

[4] McIntyre, M. E., Schumacher, R. T., Woodhouse, J., On the oscillations of musical instruments. J. Acoust. Soc. Amer. **74** [1983], 1325–1345.

[5] Woodhouse, J., On the playability of violins, Part 1 Reflection functions. Acustica **78** [1993], 125–136.

[6] Woodhouse, J., On the playability of violins, Part 2 Minimum bow force and transients. Acustica **78** [1993], 137–153.

[7] Smith, J. H., Stick-slip vibration and its constitutive laws. Doctoral dissertation, University of Cambridge [1990].

[8] Schelleng, J. C., The violin as a circuit. J. Acoust. Soc. Amer. **35** [1963], 326–338.

[9] Helmholtz, H., On the sensations of tone. Dover, New York 1954 (English translation of the German edition of 1877).

[10] McIntyre, M. E., Schumacher, R. T., Woodhouse, J., Aperiodicity in bowed-string motion. Acustica **49** [1981], 13–32; see also Acustica **50** [1982], 294–295.

[11] Woodhouse, J., On the stability of bowed string motion. Acustica **79** [1993], 73–90.

[12] McIntyre, M. E., Woodhouse, J., On the fundamentals of bowed-string dynamics. Acustica **43** [1979], 93–108.

[13] Schelleng, J. C., The bowed string and the player. J. Acoust. Soc. Amer. **53** [1973], 26–41.

[14] Cremer, L., The physics of the violin. MIT Press, Cambridge MA, USA 1985.

[15] Krigar-Menzel, O., Raps, A., Über Saitenschwingungen. Ann. Phys. Chem. **44** [1891], 623.

[16] Weinreich, G., Caussé, R., Elementary stability considerations for bowed-string motion. J. Acoust. Soc. Amer. **89** [1991], 887–895.

[17] Schumacher, R. T., Self-sustained oscillations of the bowed string. Acustica **43** [1979], 109–120.

[18] McIntyre, M. E., Woodhouse, J., A parametric study of the bowed string: the violinist's menagerie. J. Catgut Acoust. Soc. **42** [1984], 18–21.